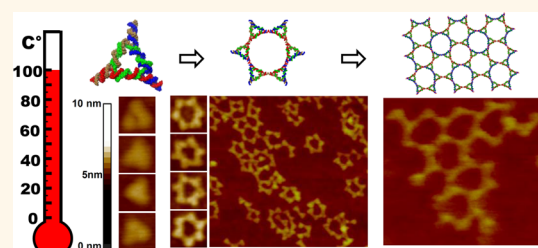


# RNA as a Boiling-Resistant Anionic Polymer Material To Build Robust Structures with Defined Shape and Stoichiometry

Emil F. Khisamutdinov, Daniel L. Jasinski, and Peixuan Guo\*

Nanobiotechnology Center, Markey Cancer Center, and Department of Pharmaceutical Sciences, College of Pharmacy, University of Kentucky, Lexington, Kentucky 40536, United States,

**ABSTRACT** RNA is a polyribonucleic acid belonging to a special class of anionic polymers, holding a unique property of self-assembly that is controllable in the construction of structures with defined size, shape, and stoichiometry. We report here the use of RNA as polymers to fabricate boiling-resistant triangular nanoscaffolds, which were used to construct hexagons and patterned hexagonal arrays. The RNA triangular scaffolds demonstrated promising potential to construct fluorogenic probes and therapeutic agents as functionalization with siRNA, ribozyme, folate, and fluorogenic RNA aptamers revealed independent functional activity of each RNA moiety. The ribozyme was able to cleave hepatitis genomic RNA fragments, the siRNA silenced the target genes, and all fluorogenic RNA aptamers retained their fluorescence emission property. The creation of boiling-temperature-resistant RNA nanoparticles opens a new dimension of RNA as a special polymer, feasible in industrial and nanotechnological applications.



**KEYWORDS:** RNA nanotechnology · 3WJ motif · RNA nanoparticles · anionic polymer · thermostable RNA · nanobiotechnology · RNA therapeutics · RNA polymer

The necessity for more robust, safe, and efficient products for pharmaceutical, medical, electronic, and biomaterial applications has increased over the years. The exploration of novel materials has become a fundamental research area with an emphasis on the generation of novel devices at the nanoscale for enhanced delivery of drugs, sensitive probes, and tissue engineering scaffolds. Among these, polymers are of particular interest for a variety of applications, as these systems/devices comprehensively demonstrate improved thermostability, chemical stability, strength, flexibility, biocompatibility, biodegradability, favorable pharmacokinetics and pharmacodynamics, low immunogenicity, and stimuli responsiveness.<sup>1–6</sup> However, one major disadvantage of chemical polymers is the difficulty in controlling the size, shape, and stoichiometry of the polymer product. The polymerization course is generally a random aggregation process. RNA is a natural polymer that has a predictable and

controllable self-assembly property to generate structures with defined size, shape, and stoichiometry.<sup>7–12</sup> Notably, triangular and square RNA structures have been constructed and experimentally confirmed by native PAGE.<sup>13–21</sup> Consequently, RNA nanotechnology<sup>19</sup> is an evolving field with enormous potential, and an alternative to the polymer field.<sup>17</sup>

The structural features of RNA motifs have been widely utilized in architectonics, an approach for rational design of 2D or 3D RNA nanoscaffolds. Thus, a variety of elegantly shaped RNA nanoassemblies have been previously obtained with a high degree of control and predictability.<sup>18–27</sup> The controlled size and 3D orientation is advantageous for biodistribution, pharmacokinetics, and toxicology properties of RNA nanoparticles.<sup>17,28</sup> For example, the pRNA of the bacteriophage phi29 has shown great promise to be used in nanomedicine to deliver functional RNAs to specific target cells.<sup>29–33</sup>

\* Address correspondence to peixuan.guo@uky.edu.

Received for review January 30, 2014 and accepted March 25, 2014.

Published online April 03, 2014  
10.1021/nn5006254

© 2014 American Chemical Society

Despite the advantages of RNA nanoparticles, such as structural and functional diversity, the presence of the hydroxyl group at 2' ribose has a dramatic effect on its properties. Even though double-stranded RNA offers improved thermal stability with base stacking and fixed C3'-endo sugar associated A-form helical structure, RNA is still amenable to RNase digestion<sup>34</sup> and can be hydrolyzed by divalent metal ions.<sup>35</sup> The lack of covalent bonds among RNA nucleotides within the 3D structure, together with reactive 2'-OH group, makes RNA relatively unstable and dissociable at ultralow concentrations. Although chemical modifications to RNA nucleotides have been shown to be useful in extending the half-life of RNA in the body, RNA secondary structure is still sensitive to denaturation.<sup>31</sup>

In a recent report, the 3WJ motif of pRNA was discovered to be unusually stable.<sup>32</sup> This property of the 3WJ was successfully used to generate highly stable RNA nanoparticles capable of carrying therapeutic RNA moieties including siRNA, ribozymes, and receptor-binding aptamers.<sup>18,33</sup> Here, we report the rational design of novel triangular-shaped RNA nanoparticles using the structural features of the pRNA-3WJ motif. The designed triangular module was found to be significantly more thermostable than the previously reported pRNA-3WJ<sup>32</sup> and 4WJ.<sup>18</sup> The triangles were resistant to boiling temperature and were used for the construction of supramolecular assemblies, delivery of RNA therapeutic moieties, and as stimuli responsive nanodevices. The main motivation was the construction of RNA triangular scaffold out of pRNA 3WJ and demonstration of its robust applicability. As such, our goal was to demonstrate that the thermodynamically stable geometry of the 3WJ can be utilized for construction of other building blocks for industrial applications. Polymers have enormous applications in industry; a new anionic polymer that can be controlled to build structures with defined shape and stoichiometry will add unexpected applications to the polymer field.

## RESULTS AND DISCUSSION

**Design of RNA Triangular Nanoparticles.** The key to building large RNA architectures is the control of turning angles. The 3D crystal structure of the 3WJ domain of phi29 pRNA<sup>36</sup> was used to manually design RNA triangular models using Swiss PDB Viewer (Figure 1A). The crystal structure of the 3WJ domain contained three short helices: H1, H2, and H3. Each helix of the 3WJ was extended with 8 nucleotides (NT). This extended pRNA-3WJ structure with three helices formed a planar shape. The importance in the outcome of this pRNA-3WJ is that the angle created between H<sub>1</sub> and H<sub>2</sub> was ~60°. Three copies of the extended 3WJs structures were as follows: H<sub>1</sub> of the first 3WJ was joined with H<sub>2</sub> of the second 3WJ. In the same manner, H<sub>1</sub> of the second 3WJ was connected to H<sub>2</sub> of the third 3WJ, and H<sub>1</sub> of the third 3WJ was joined with H<sub>2</sub> of

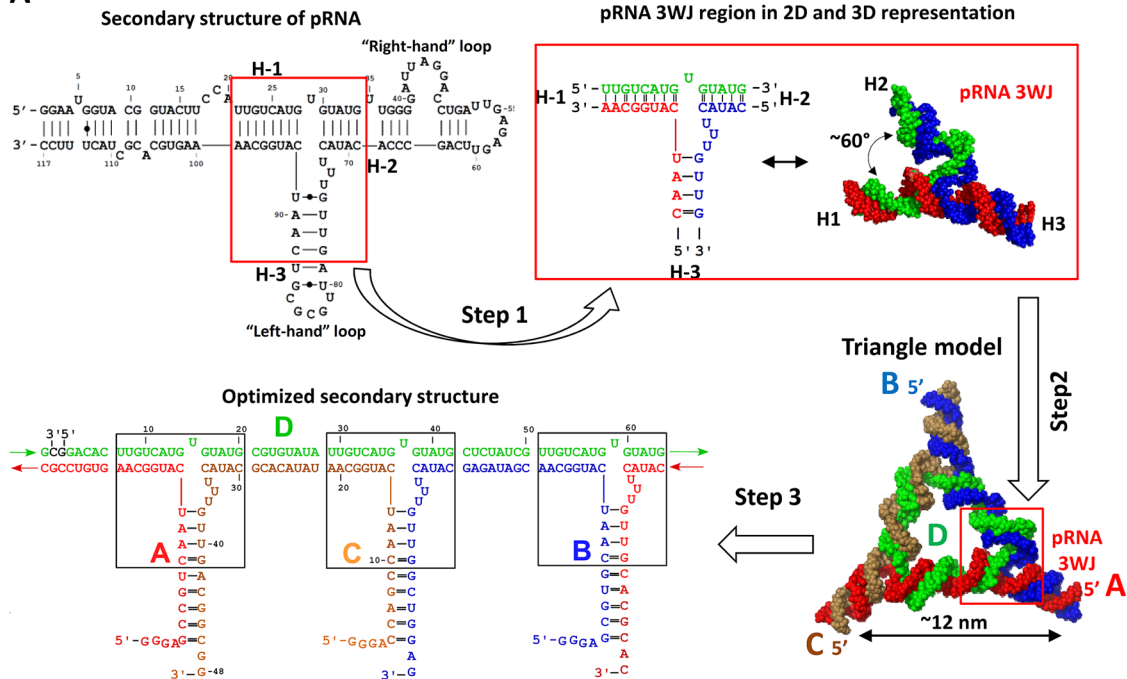
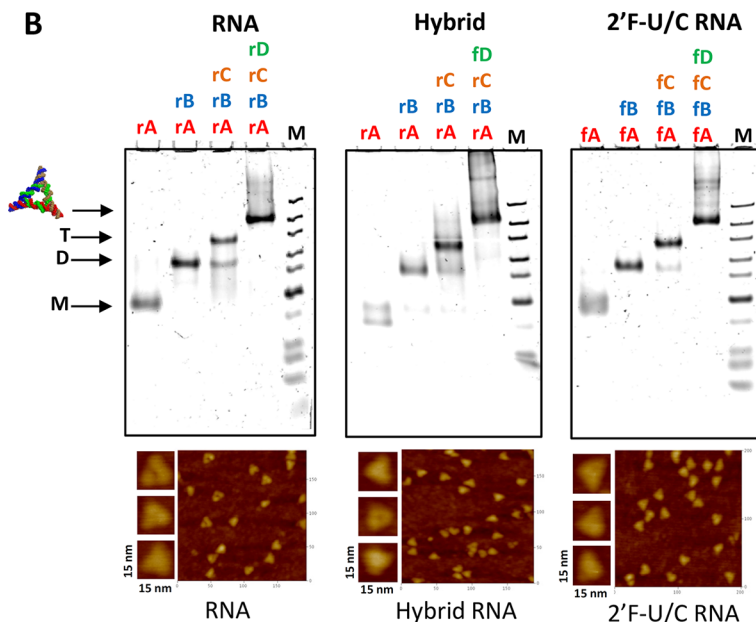
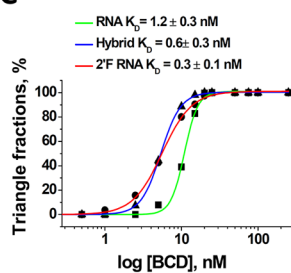
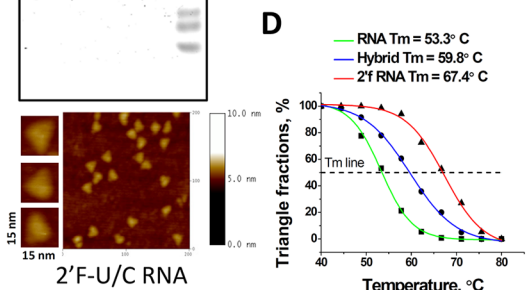
first 3WJ. Thus, a connection resulted in an equilateral triangle whose angles all equal ~60°.

The final triangle model contained four RNA strands: three short (A, B, and C) that were equivalent in length and a fourth longer strand, referred to as D, that formed the core of the triangle. The triangle nanoparticles contained three pRNA-3WJ motifs, one at each vertex (corner), that were ~12 nm in length when measured from one vertex to another. To preserve planar triangular conformation, 8 bp between 3WJ domains after the subsequent joining of H<sub>1</sub> and H<sub>2</sub> was optimal. As a result, the dihedral angle between each 3WJ was 0°. The secondary structure of the triangle was obtained by RNA sequence optimization using *mfold*.<sup>37</sup> This was done to avoid self-folding, as well as to prevent the formation of alternative secondary structures.

The designed RNA nanoparticle with an equilateral triangular shape has several advantages with which to address the needs of nanotechnology: (i) relatively small size ~12 nm, (ii) ability to carry multiple functional RNA groups simultaneously, and (iii) can be utilized in the construction of a supramolecular pattern resembling honeycombs. Several biochemical approaches including polyacrylamide gel electrophoresis (PAGE), temperature gradient gel electrophoresis (TGGE), and atomic force microscopy (AFM) were implemented to confirm the formation of the triangular structures and its functional derivative, as well as to elucidate their properties. For comparison, three different triangles, (1) an RNA triangle (rA, rB, rC, and rD); (2) a 2'F-U/C modified triangle (fA, fB, fC, and fD); and (3) a hybrid triangle (rA, rB, rC, and fD), were used in this study.

**Self-Assembly Properties of RNA Triangles.** The triangular nanoparticle stepwise self-assembly of RNA, 2'F-U/C modified RNA, and hybrid RNA was monitored by 6% native PAGE (Figure 1B). The gradually decreasing mobility of RNA species on the gel upon addition of corresponding strands indicated the formation of monomers (M), dimers (D), trimers (T), and fully assembled triangles (tetramers). The yield of RNA folding into correct triangular units was estimated to be ~90%. The AFM images of each purified fraction of tetramers further provided evidence that the assembled strands of nanoparticles had a triangular shape (Figure 1B). The measured dimensions of 3D models correlated well with those obtained by AFM images, and were within 12 nm. To confirm that all four RNA strands participated in the formation of the triangle, additional radio-assay PAGE experiments were performed (Supporting Information, Figure S1A). The resulting PAGE shows that all nanoparticles localized as a unique band on the gel with identical migration distances indicating incorporation to triangle fractions.

Since each corner of the triangle was composed of the chemically and thermodynamically stable pRNA-3WJ

**A****B****C****D**

**Figure 1. RNA triangle nanoparticles design scheme and self-assembly. (A)** Design scheme of triangular nanoparticle. Step 1, the atomic resolution structure of pRNA 3WJ motif highlighted by the rectangle was obtained and analyzed. The flexible angle  $\sim 60^\circ$  formed by H1 and H2 was used for triangle design on Swiss-PDB viewer as shown in following step. Step 2, the 3D model of triangle shape was designed by carefully joining extended helices (H1 and H2) using Swiss PDB viewer software. Step 3, the sequences and secondary structure of the triangle was obtained based on free energy sequence optimization algorithm using *mfold*. The resulting secondary structure contained four RNA strands: three identical in length (48 nt) A (red), B (blue), and C (brown), as well as longer strand D (green 66 nt). **(B)** Native PAGE (6%) showing stepwise association of individual strands into triangle fractions, RNA total strands stain in ethidium bromide (E.B.). Lane M is the DNA stepladder. The corresponding AFM images of purified triangles are shown at the bottom. **(C)** Titration curve fitting data collected from several independent experiments of RNA, 2'F-RNA, and Hybrid triangle assembly. **(D)** Thermal melting curves of RNA, 2'F-RNA, and hybrid triangles obtained from TGGE data.

motif, we further addressed the question regarding the assembly of triangles in harsh conditions, particularly in the presence of 8 M urea (Supporting Information, Figure S1C). The assembly data showed that the

formation of the 2'F-U/C modified RNA triangles in this harsh environment was highly  $Mg^{2+}$ -dependent. A very weak triangle fragment was detected at 0 mM  $MgCl_2$ ; however, at 1 mM there was a clearly visualized

triangle band; further increasing the  $Mg^{2+}$  concentration did not increase the yield of the nanoparticle. The  $Mg^{2+}$  was extremely important in stabilizing the pRNA-3WJ tertiary conformation, as demonstrated previously.<sup>36,38,39</sup> This indicates that 2'F-modified RNA strands had a tremendous affinity to assemble into triangular geometry, and that the triangle can form in the presence of the denaturing reagent. To our knowledge, this finding of RNA self-assembly in presence of 8 M urea has not been documented anywhere before.

**Comparison of Stabilities in RNA, Hybrid, and 2'F-RNA Triangular Nanoparticles.** To compare the assembly properties of the triangular nanoparticles, apparent dissociation constants ( $K_D$ ) were obtained at an equilibrium state, a parameter that directly reflects the assembly of RNA at different concentrations. The  $K_D$  value for the RNA triangle was found to be  $\sim 1.2$  nM;  $K_D$  values for hybrid and 2'F-U/C triangles were  $\sim 0.6$  and 0.3 nM, respectively (Figure 1C). Since the  $K_D$  values reflect the stabilities of individual nanoparticles, the data indicates that 2'F-nanoparticles were more stable than hybrid, and hybrid were more stable than RNA triangles.

In addition, to investigate and compare the thermostability, temperature gradient gel electrophoresis (TGGE)<sup>23,26,33</sup> studies were employed to determine the melting temperatures of the individual triangles. The melting temperatures of the triangles were determined by measuring the decrease in the yield of triangular fractions *versus* temperature. A temperature gradient was applied perpendicular to the electrical current. Initially, experiments were conducted in presence of 10 mM  $MgCl_2$  with an RNA concentration of 100 nM and no melting temperatures ( $T_M = 50\%$  triangle formed) (Supporting Information, Figure S3) were reached in the temperature range of 40–80 °C. The concentrations of the triangles were then diluted from 100 to 1 nM, which also did not result in a melting temperature determination. The TGGE system used in our experiment was not capable of heating the thermal block over 80 °C. This initial data suggests that even at 1 nM concentration triangular nanoparticles exhibit a  $T_M$  higher than 80 °C. By contrast, when the concentration of  $Mg^{2+}$  was reduced to 0.2 mM,  $T_M$  values were reached (Figure 1D), and the most stable was the 2'F-modified triangle with  $T_M = 67.4$  °C, followed by the hybrid triangle  $T_M = 59.8$  °C, and the RNA triangle  $T_M = 53.3$  °C. This data is consistent with their low  $K_D$  values. Thus, the triangular nanoparticles are extremely stable as they exhibited subnanomolar  $K_D$  and high  $T_M$ . This stability is presumably due to a synergistic effect of three thermodynamically stable pRNA-3WJ motifs. Combination of three 3WJs could lead to a added effect concerning structure stability due to the increased number of Watson–Crick base pairs and inter-domain interactions. Importantly, it has been found

that the thermostability of the triangles can be simply tuned by substituting RNA strands to 2'F-U/C and *vice versa*, or by varying  $Mg^{2+}$  concentration.

**Resistance of the RNA Nanoparticles to Boiling Temperature and in Presence of 8 M Urea.** The above data obtained by TGGE analysis suggested that the  $T_M$  of RNA triangular nanoparticles are higher than 80 °C in the presence of 10 mM  $MgCl_2$ ; thus, the triangular nanoparticles could be resistant to much higher temperatures (e.g., boiling 100 °C).

To test nanoparticle resistance to boiling temperatures, the 5'-end of the A, both RNA and 2'F-U/C, strand was [ $\gamma$ -<sup>32</sup>P]-ATP labeled, and these were then preassembled with their complementary strands. The samples were incubated for 5 min at 100 °C in presence of the competitor “cold” strands, rA or fA, ranging in stoichiometric ratios from 1:0 to 1:3 for RNA, hybrid, and 2'F-U/C triangles (Figure 2A). Quantification analysis of remaining triangle bands showed that the fraction of hybrid and 2'F-U/C RNA nanoparticles remained 100% after incubation at boiling temperature, without the presence of a competitor strand. The RNA triangle partially dissociated, but a large fraction ( $\sim 75\%$ ) still remained as an assembled component, demonstrating the resistance of triangular nanoparticles to boiling temperature.

To further evaluate and compare the stabilities of the triangles, we conducted the same boiling resistance assay but in the presence of 8 M urea. Preassembled triangles (5  $\mu$ M each in TMS buffer) were mixed with urea (8 M final concentration) and either incubated at room temperature (RT) for 30 min or heated to 100 °C followed by cooling on ice. The resulting PAGE demonstrated that all triangles were resistant to urea as individual bands corresponding to triangles were observed, shown in Figure 2B. Heating in presence of urea, however, destabilized the triangular species (Figure 2B) to an insignificant extent. This, in addition to  $K_D$  and  $T_M$ , demonstrated the extraordinary stability properties of the RNA, hybrid, and 2'F-U/C RNA triangles.

**Multipurpose RNA Triangular Nanobricks.** It is of particular importance to demonstrate the potential applicability of the triangular RNA nanoscaffolds. As such, we raised the question whether incorporated functional RNA moieties, including RNA fluorogenic aptamers, and therapeutic RNA molecules would fold into their functional 3D structures with preserved functionalities resulting in multifunctional RNA nanoparticles. Furthermore, we tested the triangle's use as a building block for the construction of supramolecular structures.

**Triangles as Fluorogenic Reporters.** The concept of multifluorescent nanodevice fabrication *via* triangular nanoscaffold assembly was demonstrated using two different fluorogenic RNA aptamers emitting light in different spectra: MG<sup>40</sup> and SPINACH<sup>41</sup> as well as 3'-end Cy3 labeled ssRNA. The triphenylmethane

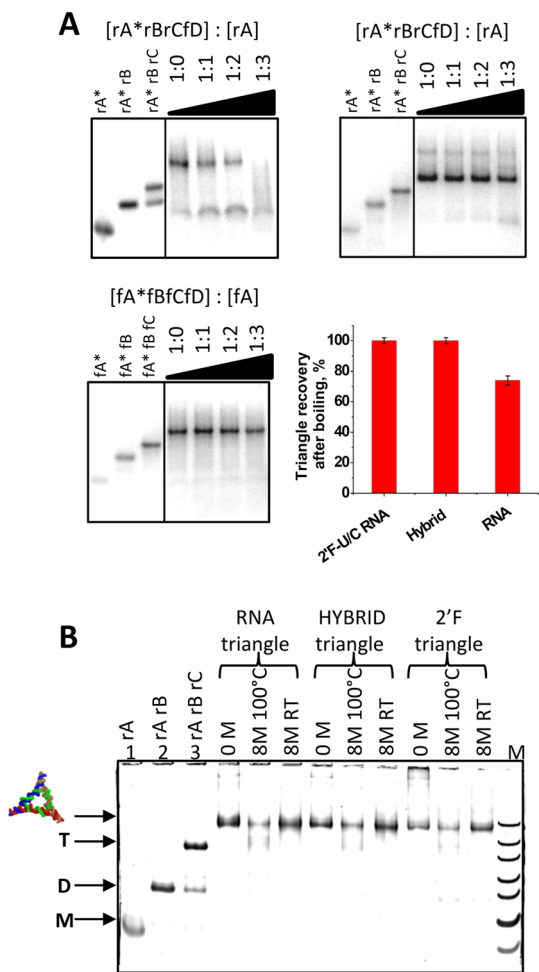


**Figure 2. Boiling temperature and urea resistance assay.** (A) The boiling temperature effects on stability of RNA, hybrid, and 2'F-RNA triangles evaluated by 6% native PAGEs. Fixed concentrations of  $^{32}\text{P}$  ATP-labeled [rA\*], rB, rC, rD], [rA\*, rB, rC, 2'F-D], and [2'F-A\*, 2'F-B, 2'F-C, 2'F-D] triangles were incubated with unlabeled rA or 2'F-A strands at ratios from 1:0 to 1:3 for 5 min at 100  $^{\circ}\text{C}$ . The quantified fractions of remaining triangles obtained from three independent experiments are shown on bottom left. (B) Effect of 8 M UREA on stability of triangles. The 8% polyacrylamide gel was cast in 1  $\times$  TB buffer, and the RNA bands were visualized by total RNA stain in E.B.

(MG) and 3,5-difluoro-4-hydroxybenzylidene imidazolinone (DFHBI) dyes exhibit no fluorescence in solution when in an unbound state. Upon binding to their aptamers, the fluorescence increases drastically; however, to achieve this, the aptamers must fold correctly. RNA and hybrid triangles were used in this study, but not 2'F-nanoparticles because the original MG aptamer sequence was not generated by the 2'F nucleotides.

The RNA fluorogenic nanoparticles were designed by fusing the corresponding MG and SPINACH aptamers, as well as the complementary RNA sequence, to the Cy3 labeled ssRNA into the triangle RNA strands (Supporting Information, Figure S5A). To verify that the assembled nanoparticles were functional, the fluorescence assay was performed directly on native PAGE (Figure 3A). For convenience, the resulting fluorescence

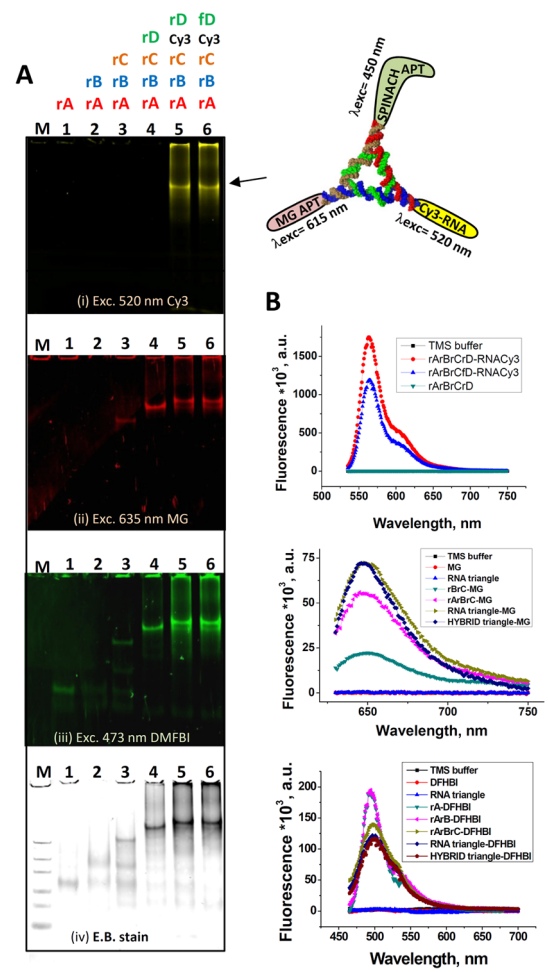


**Figure 3. Construction of multifunctional fluorogenic RNA triangles harboring MG and SPINACH RNA aptamers and Cy3-labeled DNA.** (A) Assembly of fluorogenic triangles evaluated on 6% native PAGE. Gel fluorescence assay from top to bottom: (i) gel was directly scanned using Cy3 channel, then stained simultaneously in solution containing DFHBI and MG dyes (5  $\mu\text{M}$ ), and scanned using MG channel (ii) and SPINACH channel (iii). (iv) Gel was stained in E.B. for total RNA visualization. (B) Fluorescence assay in solution (TMS buffer) of corresponding RNA and hybrid triangles. The excitation wavelengths used were  $\lambda_{\text{exc}}$  Cy3 = 520 nm,  $\lambda_{\text{exc}}$  MG = 615 nm,  $\lambda_{\text{exc}}$  SPINACH = 450 nm. (C) AFM images of fluorogenic RNA and hybrid triangles. A curve like tail at one of the corners is the signature of the SPINACH aptamer sequence.

of SPINACH aptamer is shown in green color, MG in red, and Cy3 in yellow. Thus, we are able to detect emission of different RNA aptamers as well as the Cy3 dye within the same triangular species by tuning excitation wavelength. This indicates that the MG and SPINACH aptamers fused into triangular nanoparticles retain their structure and functionality.

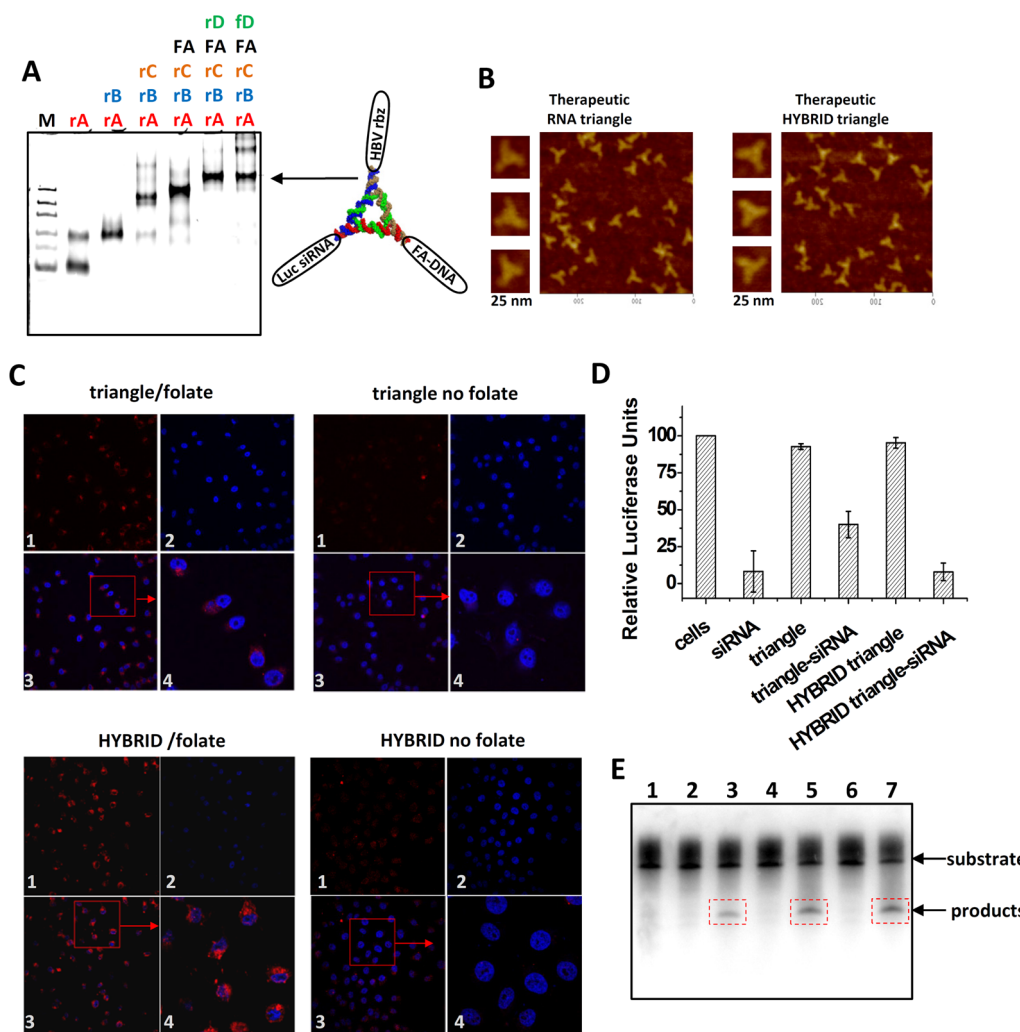


**Figure 4.** Assay of multifunctional therapeutic RNA triangles harboring ribozyme, siRNA, and folate conjugated ssDNA. (A) Assembly of the RNA and hybrid triangles evaluated in 6% native PAGE, stained in E.B. for total RNA visualization (B) AFM images of corresponding therapeutic RNA and hybrid triangles. (C) *In vitro* targeting assay. Confocal images showing the targeting of RNA nanoparticles to folate receptor (FR) positive KB cells by colocalization (overlap, 3; magnified, 4) of Cy5 labeled triangular RNA nanoparticles (red, 1) and nuclei (blue, 2). (D) Luciferase silencing assay demonstrated function of the triangles harboring siRNA (12.5 nM). (E) Assessment of RNA and hybrid triangles for HBV ribozyme catalytic cleavage activity in 10% denaturing PAGE. Lanes: 1, HBV ribozyme RNA substrate; 2, RNA substrate incubated with inactive pRNA HBV ribozyme; 3, RNA substrate incubated with pRNA HBV ribozyme; 4, RNA substrate incubated with RNA triangle; 5, RNA substrate incubated with hybrid triangle; 6, RNA substrate incubated with hybrid HBV ribozyme triangle; 7, RNA substrate incubated with hybrid HBV ribozyme triangle.

Emission properties of the fluorogenic triangles in solution were also measured. The fluorescence spectra obtained for individual RNA and hybrid triangles in the presence of 1  $\mu$ M MG and DFHBI dyes, as well as for Cy3 labeled ssRNA, support PAGE experiments (Figure 3B). Fused SPINACH and MG RNA aptamers retained their capacity to bind DFHBI and MG dyes, as demonstrated by their fluorescence emissions suggesting functional properties of triangular nanoparticles.

Furthermore, the AFM images confirmed the triangular shape of the assembled fluorogenic nanoparticles (Figure 3C). Interestingly, one corner of RNA and hybrid triangles had a distinct curve-like tail, which most likely resulted from the shape of the SPINACH RNA aptamer as its sequence was large enough to be

detected alone by AFM, compared to MG and Cy3 functionalities.

These results indicate that the RNA and hybrid triangular nanoparticles can be multifunctionalized with different RNA aptamers simultaneously and the emission signals can be then tuned by applying different excitation wavelength. This demonstrates the robust potential of fluorogenic triangular nanoparticles as image reporter devices and also a potential in computer “logic gate” operations.<sup>43</sup>

**RNA Triangular Nanoscaffolds as Therapeutic Agents.** The RNA therapeutics research focuses on discovering various approaches to introduce small noncoding RNAs including siRNA, miRNA, ribozyme and/or reporter genes into living cells.<sup>44</sup> Thus, the primary goal was

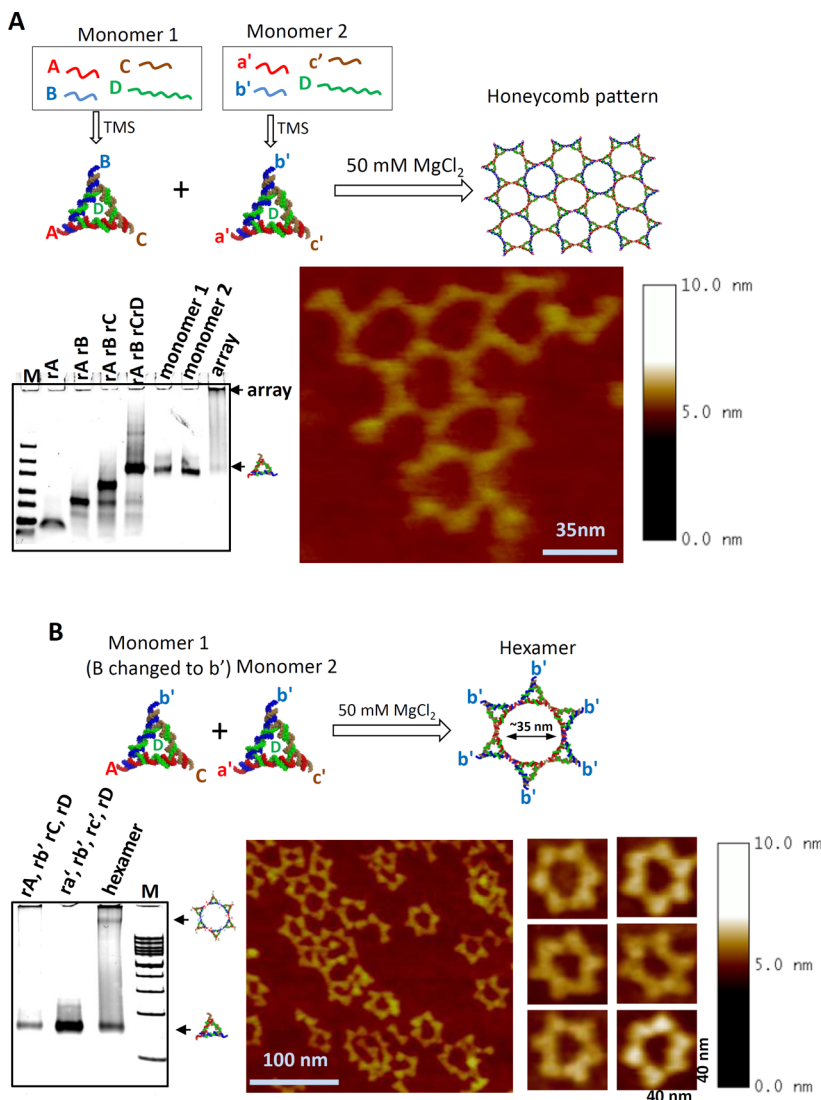


**Figure 5. Fabrication of structured honeycomb arrays using RNA triangles. (A)** Schematic diagram of the experimental design; two monomers interact with each other using sticky nucleotides: A–a', B–b', and C–c'. Native 6% PAGE and AFM images confirm the formation of honeycomb triangle pattern. **(B)** Formation of hexamer unit of honeycomb pattern. The B strand in monomer 1 was substituted for its complementary b' strand to prevent poly array formation. The 6% native PAGE shows the formation of a hexamer that was further evaluated by AFM. Lane M on the native PAGE is the 100 bp DNA ladder (Fermentas Life Sciences).

to deliver these RNA functionalities to specific targets *in vivo* via stable RNA scaffolds to prevent the degradation of individual functional RNA components. Therefore, the RNA and hybrid triangles were further designed to harbor functional therapeutic moieties, including luciferase siRNA to target the firefly luciferase gene,<sup>18</sup> a Hepatitis B virus cleaving ribozyme, and a short DNA strand containing folate (FA) ligand<sup>29</sup> (Supporting Information, Figure S5B). In addition, the core RNA or 2'F-U/C D strands were whole chain labeled with Cy5 to serve as reporter component in cellular uptake. The assembly of such therapeutic triangles was confirmed by native PAGE (Figure 4A) and further evaluated by AFM (Figure 4B).

Next, the function of each RNA moiety was assayed individually to confirm that each was able to function

while bound to the triangular scaffold. The FA incorporated triangles were assayed based on their ability to facilitate cancer cell targeting, as previously reported.<sup>45</sup> The “naked” triangles with no FA conjugated RNAs served as negative controls. Confocal imaging indicated binding of the triangular nanoparticles harboring FA and their entry into the targeted cells, as demonstrated by the colocalization and overlap of the fluorescent RNA nanoparticles (red) and nuclei (blue), shown in Figure 4C. The nonspecific cell entry is not significant since the nanoparticle size is about 13 nm, which is larger than the 23 nt double-stranded siRNA itself. In addition, RNA is negatively charged. The larger size will reduce the random entry rate of the negatively charged and ligand-free RNA nanoparticles to enter normal cells that do not contain specific receptors.

Figure 4D demonstrates the silencing function of the triangular nanoparticles containing siRNA for firefly luciferase. The low ratio of firefly to renilla luciferase expression relative to a scrambled RNA control indicated proper siRNA functioning by the triangle nanoparticles. The HBV ribozyme on the nanoparticles was able to cleave the 135 nt genomic RNA substrate (Figure 4E), indicating that ribozyme retained its native conformation and function.

**Organizational Power of Triangular Nanobricks for Patterned 2D Arrays.** The bottom-up spatial organization of nucleic acid based polymers is the key intermediate in the development of molecular electronics and tissue engineering. The application of sticky ends has been shown in fabrication of 2D and 3D structured arrays, as well as in complex 3D RNA nanostructures.<sup>17,19,21,23,46–48</sup> To reveal the potential feasibility of triangle nanoparticles in 2D supramolecular construct formations, the triangles were functionalized at their corners with sticky ends containing 6-nt. Swiss-PBD program was used to model the 2D supramolecular complex, and final sequences for monomer 1 and 2 were obtained using *mfold* (Supporting Information, Figure S5C). By using three branches of the triangles, we were able to produce 2D honeycomb-like arrays evidenced by native PAGE (Figure 5A). A 1:1 ratio of monomer 1 and monomer 2 with three sticky ends was used to construct the honeycomb-like array structures. The overall topology was investigated by AFM in air in presence of 50 mM MgCl<sub>2</sub> solution. This Mg<sup>2+</sup> concentration was found to be necessary to stabilize the overall honeycomb geometry as only 6 interacting nucleotides were introduced. The predicted and observed honeycomb-like architectures were in remarkable agreement with each other. The central cavity has an overall size of ~35 nm. Similarly, upon inactivation of one corner of

the triangles, we were able to construct a single hexamer unit of the honeycomb array (Figure 5B). The B strand of monomer 1 was replaced by b' strand from monomer 2; thus, the interaction of B–b' corner was blocked preventing the supramolecular complex formation. Again, utilizing a 1:1 ratio of monomer 1 to monomer 2, with 2 sticky ends, a single hexamer unit was assembled.

Thus, the concept of sticky end conjugation was successfully applied to the thermostable RNA triangles. This opens a new route to organize different molecular components with high precision, to generate nanochips, nanocircuits, and nanodevices with potential applications in computer and material sciences, nanotechnology, and nanomedicine.

## CONCLUSION

The thermodynamically stable pRNA-3WJ tertiary motif of the bacteriophage phi29 DNA packaging motor can be used to engineer programmable, self-assembling RNA nanoscaffolds with a defined triangular shape. In addition to subnanomolar  $K_D$  values and high melting temperatures, the triangular nanobricks were also shown to be resistant to boiling. The 2'-F-U/C modified RNA triangle showed exceptional stability, as it self-assembled in 8 M urea solution. These stable nanomaterials were feasible as scaffolds to harbor multiple RNA functionalities, as demonstrated by multifunctionalization assays with fluorogenic RNA aptamers, as well as therapeutics moieties. Exceptionally stable triangle scaffolds are perfect materials to build supramolecular complexes: hexamers or honeycomb structured arrays. This work paves the way toward production of highly stable RNA anionic polymer for potential application in technological needs alternative to the chemical polymers.

## MATERIALS AND METHODS

**Design, Preparation, And Assembly of RNA Triangles.** The three-dimensional structure of the pRNA 3WJ core motifs were obtained from a previous report.<sup>36</sup> Each “arm” of 3WJ was manually extended with 8 bp helices using Swiss-PDB Viewer. The resulting 3D atomic model was primarily used for triangular pRNA shape as follows: H<sub>1</sub> of first 3WJ was connected to H<sub>2</sub> of the second structure, H<sub>1</sub> of the second 3WJ was connected to H<sub>2</sub> of the third structure, and H<sub>1</sub> of the third 3WJ was connected to H<sub>2</sub> of the first 3WJ. The triangle model was made planar by twisting the preformed dihedral angle between H<sub>1</sub> and H<sub>2</sub>.

Synthetic DNA molecules coding for the antisense sequence of the triangle RNA strands were purchased from IDT DNA ([www.idtdna.com](http://www.idtdna.com)) and amplified by PCR using primers containing the T7 RNA polymerase promoter. PCR products were purified using the QiaQuick PCR purification kit (Qiagen Sciences, Germantown, MD). RNA molecules were prepared by *in vitro* transcription using T7 RNA polymerase. Modified RNA strands (2'-deoxy-2'-fluoro) were synthesized by *in vitro* transcription with the mutant Y639F T7 RNA polymerase<sup>50</sup> using the 2'-F modified dCTP and dUTP (Trilink).<sup>51</sup> When necessary, RNA strands were labeled at the 5'-end with [<sup>32</sup>P] ATP (PerkinElmer)

or were whole body labeled using Label IT siRNA Tracker Intracellular Localization Kit, Cy3TM or Cy5TM (Mirus Bio LLC).

The triangles assembly was achieved by mixing equimolar RNA strands (1  $\mu$ M) in TMS (50 mM Tris, pH 8.0, 100 mM NaCl, and 10 mM MgCl<sub>2</sub>) buffer by heating to 94 °C and slow cooling (over 1 h) to +4 °C, or by incubating RNA strands in TMS buffer at 37 °C for 30 min. Alternatively, the four individual DNA templates can be mixed at equimolar concentrations in transcription buffer and assembled co-transcriptionally in one step (data not shown), as previously described.<sup>49</sup>

**Native-PAGE,  $T_m$  and  $K_D$  Measurements.** The triangular constructs were assembled as indicated above, and 6 $\times$  loading dye (80% sucrose, 0.01% bromophenol blue, 0.01% xylene cyanol) was added to each RNA sample prior to loading on native gels. All native gels were run at +4 °C at 90 V for 3 h. Ethidium bromide solution was used for total RNA, hybrid, and 2'-F-U/C stain. The corresponding bands were visualized using Typhoon imager (GE) with the emission centered at 570 nm. The gels containing fluorogenic triangles were stained in a mixture of MG and DFHBI dyes (5  $\mu$ M) for 10–20 min and visualized by Typhoon at the SPINACH  $\lambda_{exc}$  = 473 nm and MG-apt  $\lambda_{exc}$  = 635 nm. The gels containing Cy3 and Cy5 labeled triangles were visualized on Typhoon with  $\lambda_{exc}$  = 532 nm and  $\lambda_{exc}$  = 635 nm. The gels

containing 5'-end radiolabeled RNA strands were vacuum-dried and exposed to a phosphoimager screen overnight prior scanning with the Typhoon imager.

Apparent equilibrium constants of dissociation ( $K_D$ ) for triangles were determined in TMS buffer according to a previously described procedure.<sup>49</sup> Briefly, the quantified triangle fractions (f) were plotted versus the total concentration (Ct) of the RNA, hybrid, or 2'f-U/C strands. The nonlinear curve fitting was applied to the data from several independent experiments using Origin 8.0 software. The general equilibrium equation for multistrand nucleic acid components was used according to<sup>52</sup>

$$K_D = \frac{\left(\frac{Ct}{2n}\right)^{n-1} \times (1-f)^n}{f} \quad (1)$$

where  $n = 4$  (four RNA strands).

All gels were quantified using ImageJ software. Equal-sized boxes were drawn around the bands corresponding to the triangle fractions. The yield for each RNA, hybrid, or 2'f-modified triangles was calculated by dividing the corresponding quantified value for triangles by the total sum of the values for all monomers, dimers, and trimers present in the quantified lane.

Melting temperatures of the triangular nanoparticles were calculated based on native TGGE as previously described.<sup>33,46</sup> Analysis was performed using in both 10 and 0.2 mM MgCl<sub>2</sub>; a linear temperature gradient from 40 to 80 °C was applied perpendicular to the electric field (Supporting Information, Figures S3 and S4). Gels were run for 1.5 h, at 30 W. Initially, TMS buffer was used in the concentration dependent study of varying RNA concentrations tested (100–1 nM) resulting in no transition curve. For these studies, a TGGE system (Biometra GmbH, <http://www.biometra.com/2440.html>) was employed allowing for the observation of the melting RNAs.

**Boiling-Resistance Assay.** The 5'-end [ $\gamma$ -<sup>32</sup>P] ATP labeled A and 2'F-U/C A strands were preassembled with their complementary strands at equimolar concentrations. The samples then were incubated for 5 min at 100 °C in presence of the competitor "cold" strands A or 2'F-U/C A ranging from 1:0 to 1:3 stoichiometric ratios. This time was sufficient for the temperature to spread evenly across 10  $\mu$ L of total RNA volume. The boiling was stopped by immediately freezing the RNA samples on dry ice to prevent the refolding of any dissociated RNA products. The samples were then thawed on ice prior to subjecting them to a native PAGE equilibrated at +4 °C to minimize any reassembly processes.

**Fluorescence Measurements.** Native 6% PAGE was used to detect the fluorescence emission of fluorogenic nanoparticles. To achieve this, first we recorded the emission of Cy3-RNA incorporated strand with  $\lambda_{exc}$  centered at 532 nm on Typhoon fluorescence scanner. Then, the gel was stained simultaneously in a mixture of 5  $\mu$ M MG and 5  $\mu$ M DFHBI and scanned for the MG-apt fluorescence,  $\lambda_{exc}$  centered at 635 nm, and for SPINACH-APT fluorescence  $\lambda_{exc}$  centered at 473 nm. After images were recorded at different excitation wavelengths, the total RNA stain in E.B. solution was performed to detect all RNAs in the gel (Figure 3A, bottom).

Fluorescence emission in solution was measured as previously reported.<sup>32</sup> Briefly, assembled triangular nanoparticles (0.2  $\mu$ M) harboring MG and SPINACH aptamers in TMS buffer were mixed with MG (2  $\mu$ M) or with DFHBI (2  $\mu$ M) (Lucerna, Inc., <http://www.lucernatechnologies.com>) and incubated at room temperature for 30 min (Figure 4D). Fluorescence was measured using a fluorospectrophotometer (Horiba Jobin Yvon), excited at 450 nm (465–750 nm scanning for emission) for SPINACH and 615 nm (625–750 nm scanning for emission) for MG dyes. The Cy3 emission in range of 535–750 nm was detected using excitation wavelength of 520 nm.

**AFM Imaging.** RNA was imaged using specially modified mica surfaces (APS mica)<sup>18,32,33,53,54</sup> with a MultiMode AFM NanoScope IV system (Veeco/Digital Instruments, Santa Barbara, CA), operating in tapping mode.

**HBV Ribozyme Activity Assay.** HBV ribozyme activity assay was conducted similarly to that described previously.<sup>29</sup> Briefly, HBV RNA substrate was 5'-end radiolabeled with [ $\gamma$ -<sup>32</sup>P] ATP and incubated with the RNA triangle conjugated HBV ribozyme

or hybrid triangle conjugated ribozyme at 37 °C for 60 min in a buffer containing 20 mM MgCl<sub>2</sub>, 20 mM NaCl, and 50 mM Tris-HCl (pH 7.5). The pRNA/HBV ribozyme served as a positive control, and a pRNA/HBV disabled ribozyme was used as a negative control (Supporting Information Table S1).<sup>29</sup> The cleaved fragments were analyzed by autoradiography.

**In Vitro Binding and Entry of RNA Nanoparticles into Targeted Cells.** KB cells (ATCC) were seeded  $1 \times 10^4$  per well into chambered glass coverslips for 24 h proliferation in FA-free 1640 medium overnight and treated with 200 nM various Cy5 labeled triangles in the same medium, which included (i) RNA triangles harboring a DNA-FA ligand, (ii) control RNA triangles no DNA-FA ligand, (iii) hybrid RNA triangles harboring DNA-FA ligand, (iv) control hybrid RNA triangles DNA-FA ligand, and (v) cell only at 37 °C for 4 h followed by washing with precooled PBS. The cells were then fixed with 4% paraformaldehyde for 20 min and incubated with DAPI (invitrogen) for 24 h at room temperature. The cells were then assayed for binding and cell entry using Olympus FV1000 Confocal Microscope.

**Assay for the Silencing of Luciferase Genes in Cancer Cell Model.** KB cells, which express firefly luciferase (KB-Luc), were plated at 10 000 cells/well in a 96-well black plate (Corning Life Sciences; Tewksbury, MA) overnight and transected with triangular nanoparticles (12.5 nM) and a positive Survivin siRNA control (Ambion, Inc.) using lipofectamine 2000 (Invitrogen) for 24 h. d-Luciferin potassium salt (Research Products International Corp., Mount Prospect, IL) was dissolved in sterile PBS to make a stock solution of 10 mg/mL; the cell culture media was removed before addition of 100  $\mu$ L of a 300  $\mu$ g/mL solution of d-luciferin in PBS. Plates were incubated at 37 °C for 5 min before imaging. The IVIS Spectrum system was used for *in vitro* imaging of cells in 96-well plates. For quantification of the detected light, regions of interest were drawn by using Living Image 3.1 software, and the photon counts per second from each well were recorded and plotted. Cell numbers were quantified by staining with sulforhodamine B assay (Geno Technology, St. Louis, MO) as described previously (4WJ).

**Construction of 2D Structured Arrays.** Individual monomers were assembled by incubation at 37 °C for 30 min in TMS buffer. The resulting triangles were further purified by native 6% PAGE. The pure nanoparticles were mixed at equimolar concentrations (0.5  $\mu$ M) in Tris-HCl, pH 8.0 buffer, containing 100 mM NaCl and 50 mM MgCl<sub>2</sub>. The high [Mg<sup>2+</sup>] concentration is found to be necessary to stabilize the intermolecular interaction of 6 nt sticky ends. The resulting mixture was annealed from 50 to 4 °C overnight prior to native PAGE and AFM analysis. The hexameric structure was achieved in the same manner.

**Conflict of Interest:** The authors declare the following competing financial interest(s): P.G. is a cofounder of Kylin Therapeutics, Inc. and Biomotor and RNA Nanotechnology Development Corp. Ltd.

**Acknowledgment.** We thank Jeannie Haak for assistance in manuscript preparation and Luda Shlyakhtenko for AFM imaging at the Nanoimaging Core Facility supported by the NIH SIG program and the UNMC Program of ENRI to Yuri Lyubchenko. The research was supported by NIH grants EB003730 and CA151648. Funding to Peixuan Guo's Endowed Chair in Nanobiotechnology position is by the William Fairish Endowment Fund.

**Supporting Information Available:** Table of RNA sequences; figures of assembly of triangles in different conditions, equilibrium dissociation assay; TGGE profiles taken in TMS buffer; melting temperatures of triangles taken at 0.2 mM MgCl<sub>2</sub>, secondary structures of RNA functional triangles. These materials are available free of charge via the Internet at <http://pubs.acs.org>.

## REFERENCES AND NOTES

1. Holzerny, P.; Ajdin, B.; Heusermann, W.; Bruno, K.; Schuleit, M.; Meinel, L.; Keller, M. Biophysical Properties of Chitosan/SiRNA Polyplexes: Profiling the Polymer/SiRNA Interactions and Bioactivity. *J. Controlled Release* **2012**, *157*, 297–304.

2. Bruno, K. Using Drug-Excipient Interactions for SiRNA Delivery. *Adv. Drug Delivery Rev.* **2011**, *63*, 1210–1226.
3. Mehra, N. K.; Jain, A. K.; Lodhi, N.; Raj, R.; Dubey, V.; Mishra, D.; Nahar, M.; Jain, N. K. Challenges in the Use of Carbon Nanotubes for Biomedical Applications. *Crit. Rev. Ther. Drug Carrier Syst.* **2008**, *25*, 169–206.
4. Kesharwani, P.; Gajbhiye, V.; Jain, N. K. A Review of Nanocarriers for the Delivery of Small Interfering RNA. *Biomaterials* **2012**, *33*, 7138–7150.
5. Cheong, W. J.; Ali, F.; Choi, J. H.; Lee, J. O.; Yune, S. K. Recent Applications of Molecular Imprinted Polymers for Enantio-Selective Recognition. *Talanta* **2013**, *106*, 45–59.
6. Pillay, V.; Seedat, A.; Choonara, Y. E.; du Toit, L. C.; Kumar, P.; Ndesendo, V. M. A Review of Polymeric Refabrication Techniques to Modify Polymer Properties for Biomedical and Drug Delivery Applications. *AAPS PharmSciTech* **2013**, *14*, 692–711.
7. Guo, P. Structure and Function of Phi29 Hexameric RNA That Drive Viral DNA Packaging Motor: Review. *Prog. Nucleic Acid Res. Mol. Biol.* **2002**, *72*, 415–472.
8. Martineau, H. M.; Pyrah, I. T. Review of the Application of RNA Interference Technology in the Pharmaceutical Industry. *Toxicol. Pathol.* **2007**, *35*, 327–336.
9. Mallardo, M.; Poltronieri, P.; D'Urso, O. F. Non-Protein Coding RNA Biomarkers and Differential Expression in Cancers: A Review. *J. Exp. Clin. Cancer Res.* **2008**, *27*, No. 19.
10. Pellish, R. S.; Nasir, A.; Ramratnam, B.; Moss, S. F. Review Article: RNA Interference—Potential Therapeutic Applications for the Gastroenterologist. *Aliment. Pharmacol. Ther.* **2008**, *27*, 715–723.
11. Bora, R. S.; Gupta, D.; Mukkur, T. K.; Saini, K. S. RNA Interference Therapeutics for Cancer: Challenges and Opportunities (Review). *Mol. Med. Rep.* **2012**, *6*, 9–15.
12. Kang, K. N.; Lee, Y. S. RNA Aptamers: A Review of Recent Trends and Applications. *Adv. Biochem. Eng. Biotechnol.* **2013**, *131*, 153–169.
13. Bindewald, E.; Grunewald, C.; Boyle, B.; O'Connor, M.; Shapiro, B. A. Computational Strategies for the Automated Design of RNA Nanoscale Structures From Building Blocks Using NanoTiler. *J. Mol. Graphics Modell.* **2008**, *27*, 299–308.
14. Bindewald, E.; Hayes, R.; Yingling, Y. G.; Kasprzak, W.; Shapiro, B. A. RNAJunction: A Database of RNA Junctions and Kissing Loops for Three-Dimensional Structural Analysis and Nanodesign. *Nucleic Acids Res.* **2008**, *36*, D392–D397.
15. Dibrov, S. M.; McLean, J.; Parsons, J.; Hermann, T. Self-Assembling RNA Square. *Proc. Natl. Acad. Sci. U.S.A.* **2011**, *108*, 6405–6408.
16. Bindewald, E.; Afonin, K.; Jaeger, L.; Shapiro, B. A. Multi-strand RNA Secondary Structure Prediction and Nanostructure Design Including Pseudoknots. *ACS Nano* **2011**, *5*, 9542–9551.
17. Guo, P. The Emerging Field of RNA Nanotechnology. *Nat. Nanotechnol.* **2010**, *5*, 833–842.
18. Haque, F.; Shu, D.; Shu, Y.; Shlyakhtenko, L.; Rychahou, P.; Evers, M.; Guo, P. Ultrastable Synergistic Tetraivalent RNA Nanoparticles for Targeting to Cancers. *Nano Today* **2012**, *7*, 245–257.
19. Guo, P.; Zhang, C.; Chen, C.; Trottier, M.; Garver, K. Inter-RNA Interaction of Phage Phi29 PRNA To Form a Hexameric Complex for Viral DNA Transportation. *Mol. Cell* **1998**, *2*, 149–155.
20. Chen, C.; Zhang, C.; Guo, P. Sequence Requirement for Hand-in-Hand Interaction in Formation of PRNA Dimers and Hexamers to Gear Phi29 DNA Translocation Motor. *RNA* **1999**, *5*, 805–818.
21. Shu, D.; Moll, W. D.; Deng, Z.; Mao, C.; Guo, P. Bottom-Up Assembly of RNA Arrays and Superstructures As Potential Parts in Nanotechnology. *Nano Lett.* **2004**, *4*, 1717–1723.
22. Willems, A.; Schoonooghe, S.; Eeckhout, D.; De, J. G.; Grootenh, J.; Mertens, N. CD3 x CD28 Cross-Interacting Bispecific Antibodies Improve Tumor Cell Dependent T-Cell Activation. *Cancer Immunol. Immunother.* **2005**, *54*, 1059–1071.
23. Chworos, A.; Sevencan, I.; Koyfman, A. Y.; Weinkam, P.; Oroudjev, E.; Hansma, H. G.; Jaeger, L. Building Programmable Jigsaw Puzzles with RNA. *Science* **2004**, *306*, 2068–2072.
24. Jaeger, L.; Chworos, A. The Architectonics of Programmable RNA and DNA Nanostructures. *Curr. Opin. Struct. Biol.* **2006**, *16*, 531–543.
25. Jaeger, L.; Westhof, E.; Leontis, N. B. TectoRNA: Modular Assembly Units for the Construction of RNA Nano-Objects. *Nucleic Acids Res.* **2001**, *29*, 455–463.
26. Grabow, W. W.; Zakrevsky, P.; Afonin, K. A.; Chworos, A.; Shapiro, B. A.; Jaeger, L. Self-Assembling RNA Nanorings Based on RNA/II Inverse Kissing Complexes. *Nano Lett.* **2011**, *11*, 878–887.
27. Sevencan, I.; Geary, C.; Chworos, A.; Voss, N.; Jacovetty, E.; Jaeger, L. A Polyhedron Made of tRNAs. *Nat. Chem.* **2010**, *2*, 772–779.
28. Guo, P.; Haque, F.; Hallahan, B.; Reif, R.; Li, H. Uniqueness, Advantages, Challenges, Solutions, and Perspectives in Therapeutics Applying RNA Nanotechnology. *Nucleic Acid Ther.* **2012**, *22*, 226–245.
29. Hoeprich, S.; Zhou, Q.; Guo, S.; Qi, G.; Wang, Y.; Guo, P. Bacterial Virus Phi29 PRNA as a Hammerhead Ribozyme Escort To Destroy Hepatitis B Virus. *Gene Ther.* **2003**, *10*, 1258–1267.
30. Guo, S.; Tschanmer, N.; Mohammed, S.; Guo, P. Specific Delivery of Therapeutic RNAs to Cancer Cells via the Dimerization Mechanism of Phi29 Motor PRNA. *Hum. Gene Ther.* **2005**, *16*, 1097–1109.
31. Abdelmawla, S.; Guo, S.; Zhang, L.; Pulukuri, S.; Patankar, P.; Conley, P.; Trebley, J.; Guo, P.; Li, Q. X. Pharmacological Characterization of Chemically Synthesized Monomeric PRNA Nanoparticles for Systemic Delivery. *Mol. Ther.* **2011**, *19*, 1312–1322.
32. Shu, D.; Shu, Y.; Haque, F.; Abdelmawla, S.; Guo, P. Thermodynamically Stable RNA Three-Way Junctions for Constructing Multifunctional Nanoparticles for Delivery of Therapeutics. *Nat. Nanotechnol.* **2011**, *6*, 658–667.
33. Shu, Y.; Haque, F.; Shu, D.; Li, W.; Zhu, Z.; Kotb, M.; Lyubchenko, Y.; Guo, P. Fabrication of 14 Different RNA Nanoparticles for Specific Tumor Targeting without Accumulation in Normal Organs. *RNA* **2013**, *19*, 766–777.
34. Knapp, G. Enzymatic Approaches to Probing of RNA Secondary and Tertiary Structure. *Methods Enzymol.* **1989**, *180*, 192–212.
35. Regulski, E. E.; Breaker, R. R. In-Line Probing Analysis of Riboswitches. *Methods Mol. Biol.* **2008**, *419*, 53–67.
36. Zhang, H.; Endrizzi, J. A.; Shu, Y.; Haque, F.; Sauter, C.; Shlyakhtenko, L. S.; Lyubchenko, Y.; Guo, P.; Chi, Y. I. Crystal Structure of 3WJ Core Revealing Divalent Ion-Promoted Thermostability and Assembly of the Phi29 Hexameric Motor PRNA. *RNA* **2013**, *19*, 1226–1237.
37. Zuker, M. Mfold Web Server for Nucleic Acid Folding and Hybridization Prediction. *Nucleic Acids Res.* **2003**, *31*, 3406–3415.
38. Scott, W. G. RNA Structure, Metal Ions, and Catalysis. *Curr. Opin. Chem. Biol.* **1999**, *3*, 705–709.
39. Brannvall, M.; Mikkelsen, N. E.; Kirsebom, L. A. Monitoring the Structure of Escherichia coli RNase P RNA in the Presence of Various Divalent Metal Ions. *Nucleic Acids Res.* **2001**, *29*, 1426–1432.
40. Baugh, C.; Grate, D.; Wilson, C. 2.8 Å Crystal Structure of the Malachite Green Aptamer. *J. Mol. Biol.* **2000**, *301*, 117–128.
41. Paige, J. S.; Nguyen-Duc, T.; Song, W.; Jaffrey, S. R. Fluorescence Imaging of Cellular Metabolites with RNA. *Science* **2012**, *335*, 1194.
42. Afonin, K. A.; Danilov, E. O.; Novikova, I. V.; Leontis, N. B. TokenRNA: A New Type of Sequence-Specific, Label-Free Fluorescent Biosensor for Folded RNA Molecules. *Chem-BioChem* **2008**, *9*, 1902–1905.
43. Qiu, M.; Khisamutdinov, E.; Zhao, Z.; Pan, C.; Choi, J.; Leontis, N.; Guo, P. RNA Nanotechnology for Computer Design and *in Vivo* Computation. *Phil Trans R Soc A* **2013**, *371* (2000), 20120310.
44. Guo, P.; Shu, Y.; Binzel, D.; Cinier, M. Synthesis, Conjugation, and Labeling of Multifunctional PRNA Nanoparticles for Specific Delivery of SiRNA, Drugs and Other Therapeutics to Target Cells. *Methods Mol. Biol.* **2012**, *928*, 197–219.

45. Guo, S.; Huang, F.; Guo, P. Construction of Folate-Conjugated PRNA of Bacteriophage Phi29 DNA Packaging Motor for Delivery of Chimeric SiRNA to Nasopharyngeal Carcinoma Cells. *Gene Ther.* **2006**, *13*, 814–820.
46. Severcan, I.; Geary, C.; Verzemnieks, E.; Chvoros, A.; Jaeger, L. Square-Shaped RNA Particles from Different RNA Folds. *Nano Lett.* **2009**, *9*, 1270–1277.
47. Seeman, N. C. Nanomaterials Based on DNA. *Annu. Rev. Biochem.* **2010**, *79*, 65–87.
48. Seeman, N. C. DNA Engineering and Its Application to Nanotechnology. *Trends Biotechnol.* **1999**, *17*, 437–443.
49. Afonin, K. A.; Bindewald, E.; Yaghoubian, A. J.; Voss, N.; Jacovetty, E.; Shapiro, B. A.; Jaeger, L. *In Vitro Assembly of Cubic RNA-Based Scaffolds Designed in Silico*. *Nat. Nanotechnol.* **2010**, *5*, 676–682.
50. Sousa, R. Use of T7 RNA Polymerase and Its Mutants for Incorporation of Nucleoside Analogs into RNA. *Methods Enzymol.* **2000**, *317*, 65–74.
51. Liu, J.; Guo, S.; Cinier, M.; Shlyakhtenko, L.; Shu, Y.; Chen, C.; Shen, G.; Guo, P. Fabrication of Stable and RNase-Resistant RNA Nanoparticles Active in Gearing the Nanomotors for Viral DNA Packaging. *ACS Nano* **2010**, *5*, 237–246.
52. Marky, L. A.; Breslauer, K. J. Calculating Thermodynamic Data for Transitions of Any Molecularity From Equilibrium Melting Curves. *Biopolymers* **1987**, *26*, 1601–1620.
53. Lyubchenko, Y. L.; Shlyakhtenko, L. S. AFM for Analysis of Structure and Dynamics of DNA and Protein-DNA Complexes. *Methods* **2009**, *47*, 206–213.
54. Lyubchenko, Y. L.; Shlyakhtenko, L. S.; Ando, T. Imaging of Nucleic Acids with Atomic Force Microscopy. *Methods* **2011**, *54*, 274–283.